PHYSICAL REVIEW B, VOLUME 63, 155410

Experimental and theoretical analysis of the multiphonon excitation probability for Einstein-like modes in atom-surface scattering

Mubing Li,[1] J. R. Manson,[1] and Andrew P. Graham[2]
[1]*Department of Physics and Astronomy, Clemson University, Clemson, South Carolina 29634-0978*
[2]*Max Planck Institut für Strömungsforschung, Bunsenstraße 10, D-37073 Göttingen, Germany*

(Received 18 February 2000; revised manuscript received 2 November 2000; published 28 March 2001)

The probabilities of multiple excitation (multiphonon transfer) of decoupled, oscillating adsorbates on a surface via impact by an atom or molecule are discussed using a dynamical scattering model, and comparisons are made with helium scattering results for carbon monoxide adsorbed on metal surfaces. The scattering model, which contains no free adjustable parameters, is shown to predict correctly the angular dependence of the distribution of the multiphonon excitations in addition to the variation with incident energy and adsorbate frequency. Furthermore, the model is used to calculate the excitation probability of other vibrational modes that have not yet been observed using helium-atom scattering.

DOI: 10.1103/PhysRevB.63.155410 PACS number(s): 79.20.Rf, 34.50.Dy, 73.20.Mf

I. INTRODUCTION

Multiple surface-phonon excitation processes are an important step in the accommodation of impact energy in atom- or molecule-surface interactions.[1] These processes aid in the sticking of particles on the surface and are crucial to heat transfer between the gas and solid phases, particularly at high temperature and large particle mass.[2] Many studies have been performed for scattering from clean, well-ordered surfaces, particularly using helium-atom scattering (HAS), where the surface-phonon modes are dispersive, resulting in broad energy-transfer distributions.[3] On the other hand, a substantial number of HAS studies have shown that, with only a small fraction of the surface covered with adsorbed molecules or atoms, the phonon characteristics of the surface become dominated by dispersionless, Einstein-like phonon modes due to vibrations of the isolated or decoupled adsorbates.[4–7] This arises because these modes often have frequencies lower than the zone-boundary frequency of the clean surface Rayleigh and in-plane phonon branches, and so are easier to excite and annihilate during the scattering process for a large range of momentum transfers. In addition, the low frequency of these modes facilitates multiple excitation (multiphonon transfer), which manifests itself as overtones of the fundamental frequency in energy-resolved experiments.

In this paper, we investigate the angular distribution of the multiphonon energy-transfer processes involving adsorbed molecules for a range of incident conditions. A simple model containing no freely adjustable parameters is used to analyze the experimental results for carbon monoxide adsorbed on both Cu(001) and Pt(111) surfaces, for which all of the vibrational and adsorption parameters have been well characterized. The scattering model considers the momentum transferred to a diffusely scattering adsorbed molecule with a hard-core potential by assuming that the helium atom imparts a short duration impulse. In this way, very few assumptions need to be made about the shape of the adsorbate, or its interaction potential with the surface and the helium atom. Thus, the lack of significant deviations of the measured scattered intensities from the predictions of this model indicate that the details of the interaction potential are not important.

The adsorption of CO on Cu(001) (Refs. 6 and 8–11) and Pt(111) (Refs. 5 and 12–14) has been extensively studied and the vibrational frequencies and details of the scattering from isolated molecules have been measured. In both cases, at low coverage, the CO molecule adsorbs in a vertical configuration with the carbon atom closest to the surface on top of a surface atom. Of particular interest in the present case is the parallel frustrated translation mode, or *T*-mode, which has a frequency of $\hbar\omega = 4$ meV for CO/Cu(001) and $\hbar\omega = 6$ meV for CO/Pt(111), about a factor of 8–9 lower than the frequency of the next mode, which in both cases is the frustrated rotation. For comparison, the frequencies and assignments of the various modes and other useful quantities are given in Table I. In the present study, the multiple excitations of the *T*-mode are investigated for a range of incident angle and energy combinations. The angular data provide useful information on the scattering form factor, or shape of

TABLE I. Comparison of the vibrational frequencies and other physical properties of carbon monoxide adsorbed on the Cu(001) and Pt(111) surfaces.

Property	Designation	CO/Cu(001)	CO/Pt(111)
Frequencies ($\hbar\omega$)			
C-O stretch	ν_1	258 meV[a]	261 meV[b]
M-CO stretch	$\nu_2(S)$	42.8 meV[a]	58 meV[b]
CO rotation	$\nu_3(R)$	35.3 meV[a]	51 meV[c]
CO translation	$\nu_4(T)$	3.94 meV[d]	6 meV[e]
Adsorption site		On top	On top
Adsorption energy	E_{ads}	0.7 eV[f]	1.5 eV[g]
Onset of desorption	T_{des}	150 K	400 K[g]
Diffusion barrier	E_{diff}	32 meV[h]	130 meV[i]

[a] Reference 8.
[b] Reference 12.
[c] Reference 13.
[d] Reference 6.
[e] Reference 5.
[f] Reference 9.
[g] Reference 13.
[h] Reference 10.
[i] Reference 14.

the CO molecule, with respect to the hard-core incoherent scatterer used in the calculation, whereas the energy dependence focuses on the range of available overtones, which is related to the Bose and Debye-Waller factors. The differing frequencies of the CO *T*-mode vibration on Cu(001) and Pt(111) also tests the applicability of this approach.

In this paper the details of the helium scattering apparatus are presented in Sec. II followed by the experimental results in Sec. III. The scattering theory is detailed in Sec. IV and then compared with the experimental results in Sec. V. Section VI is a discussion of theoretical predictions for conditions under which the higher-energy vibrational modes might be observed, and the main conclusions are summarized in Sec. VII.

II. EXPERIMENT

The helium scattering apparatus[15] (HUGO II) has a nearly monoenergetic beam formed by supersonic expansion of gas from high pressure (up to 500 bar) through a 10-μm nozzle into a high-vacuum chamber with a pressure of $10^{-4}-10^{-3}$ Torr. The central section of the expansion is extracted using a conical skimmer with a 0.5-mm aperture and the angular divergence is subsequently refined using several differentially pumped stages. The incident beam energy is regulated via the nozzle temperature that can be varied in the range 20–450 K, producing energies from 4 to 100 meV. The helium pressure in the nozzle was optimized to give the best energy resolution, typically $\Delta E/E \approx 2\%$. For time-of-flight (TOF) experiments the beam is chopped into pulses using a mechanical chopper with pulse durations from 5 to 20 μsec before striking the crystal surface, which is mounted on a six-axis manipulator in an ultrahigh-vacuum chamber with a base pressure of less than 5×10^{-11} mbar. The helium atoms scattered from the surface at a scattering angle of $\theta_{SD}=95.76°$ with respect to the incident direction are measured using a magnetic-sector mass spectrometer mounted 1.4 m from the crystal surface. TOF spectra are measured using a homemade multichannel scaler, which is cycled using timing pulses from the chopper.

The Cu(001) and Pt(111) crystals were oriented to better than 0.25°, mechanically polished, and then cleaned *in situ* with cycles of sputtering with Ar^+ ions and annealing until a sharp He specular peak and low diffuse elastic intensities were observed. No impurities could be detected using Auger spectroscopy to within the detection limit of $\Theta\sim0.01$, measured with respect to the clean surface atom density. For most of the present CO measurements the dosage was below 0.23 langmuir ($1\ \text{langmuir}=1\ \text{L}=10^{-6}$ Torr sec) corresponding to a CO coverage of $\Theta_{CO}=0.028$, as determined by the attenuation of the specularly reflected intensity.[17] Typical measuring times for a time-of-flight spectrum were of the order of 5–30 min.

III. RESULTS

In order to investigate the intensity distribution and incident energy dependence of the multiphonon processes, a large number of TOF spectra were measured for a range of incident conditions. In particular, the CO/Cu(001) surface was studied because this system is well understood and the *T*-mode frequency has been measured in a number of studies.[6,10,11,16–19] To begin with, it is important to determine whether the CO coverage has an influence on the multiphonon intensities because effects of clustering were observed at low coverages in a recent study.[10] In Fig. 1, a series of TOF spectra, converted to energy transfer, are shown for several different coverages of CO ranging from $\Theta_{CO}=0.005$ to $\Theta_{CO}=0.088$. As the coverage increases another peak can be seen, in addition to the *T*-mode multiphonons at $\Delta E\approx\pm n\times4$ meV, $\Delta E\approx5.2$ meV. A previous study[10] indicated that this peak is due to interactions between CO molecules in close proximity, i.e., due to small CO clusters on the surface. This peak becomes significant at coverages above $\Theta_{CO}\approx0.05$ [Figs. 1(d) and 1(e)].

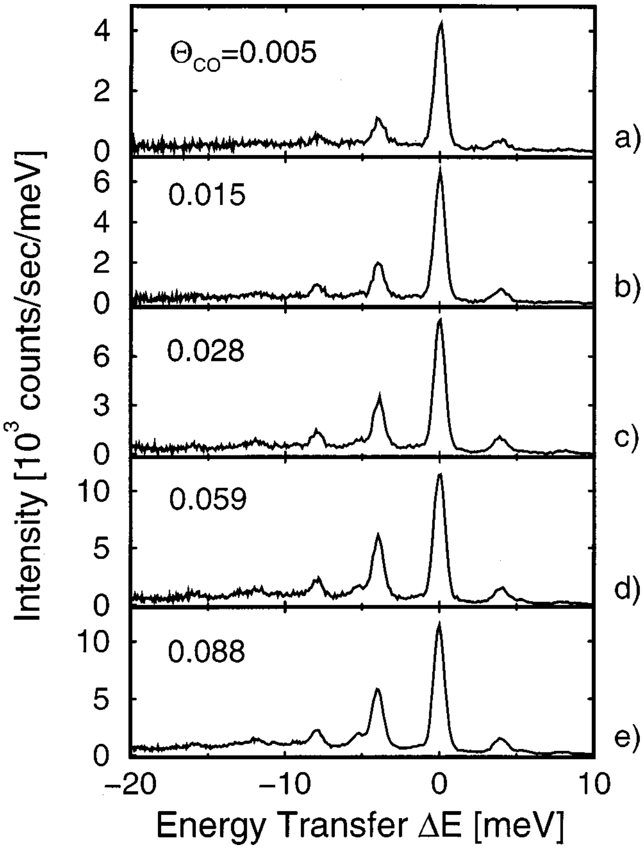

FIG. 1. A series of helium-atom scattering inelastic time-of-flight spectra, converted to an energy-transfer scale, for a range of CO coverages on Cu(001) at $T_s=50$ K. The incident energy was 40.3 meV, directed along the Cu(001) [100] azimuth at an incident angle of $\theta_i=28.2°$ in a fixed geometry in which $\theta_f=\theta_{SD}-\theta_i$ with $\theta_{SD}=95.8°$. The peaks at multiples of $\Delta E=\pm4$ meV are attributed to the excitation of the *T*-mode of isolated CO molecules adsorbed at on-top sites and become stronger with increasing coverage. (d), (e) An additional peak at $\Delta E=-5.2$ meV is visible at higher coverages above $\Theta_{CO}\approx0.05$, which is assigned to excitations of small CO clusters.

To investigate whether the clustering influences the intensity ratio between the fundamental and overtones of the *T*

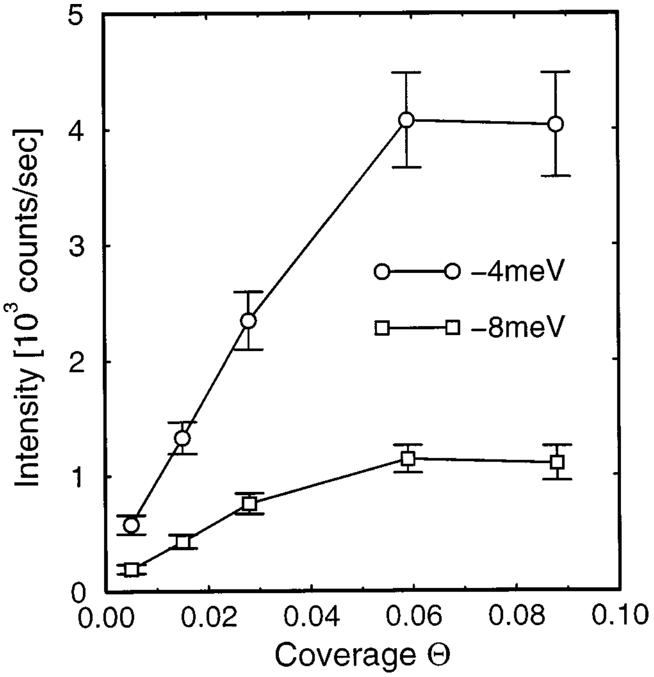

FIG. 2. T-mode fundamental ($n=-1$) and first overtone ($n=-2$) energy loss intensities as a function of surface coverage for an incident energy of 40.3 meV and an angle of $\theta_i = 28.2°$. The intensities show similar monotonic increases with a constant ratio of $I_{n=-1}/I_{n=-2} \approx 3$ up to a coverage of $\Theta_{CO} \approx 0.06$ followed by a slight intensity decrease.

mode the intensities of the fundamental energy-loss ($\Delta E = -4$ meV) and the first-overtone ($\Delta E = -8$ meV) peaks were extracted from the spectra in Fig. 1. The intensities are shown in Fig. 2. The intensities of the fundamental and first overtone exhibit a nearly linear increase with coverage up to $\Theta_{CO} \approx 0.03$, above which the rate of increase is lower with saturation occurring above $\Theta_{CO} > 0.06$. Across the whole coverage range studied the intensity ratio between the fundamental and first overtone remains approximately constant at 3. The linear increase is consistent with a simple increase in the density of scattering centers on the surface. The deviation from the linear behavior at coverages $\Theta_{CO} > 0.03$ can be interpreted as scattering involving more than one scattering center (CO molecule) due to close proximity. Thus, in order to avoid any coverage effects a coverage of less than $\Theta_{CO} \approx 0.03$ is necessary. We have used a CO coverage of $\Theta_{CO} = 0.028$ for all of the following measurements.

Figure 3 shows several typical TOF spectra measured with an incident beam energy of 66.6 meV and a surface temperature of $T_s = 50$ K for a range of incident angles for $\Theta_{CO} = 0.028$ on Cu(001). The spectra show that the total scattered intensity decreases quickly for incident angles far from the specular peak ($\theta_i = 47.9°$), as also shown in several previous studies.[18,20,21] At the same time, multiples of the fundamental T-mode frequency for CO/Cu(001) of $\hbar\omega \approx 4$ meV (Refs. 6 and 10) are observed to become much more dominant with the third overtone clearly visible at $\Delta E \approx -16$ meV.

The number of overtones excited becomes significantly larger for higher incident energies, as shown in Fig. 4. In this case, the incident angles are approximately the same but the beam energy increases from 20.0 to 83.5 meV for the same surface temperature of $T_s = 50$ K and CO coverage $\Theta_{CO} = 0.028$. At 20.0 meV three energy-loss peaks can be detected whereas at 83.5 meV the seventh energy-loss peak (sixth overtone) is clearly visible and the eighth peak is just visible above the noise. Thus, the number of excitations is not directly proportional to the incident beam energy. However, higher overtones may be hidden by the increased background level and the resulting statistical noise, which is due to the enhanced Cu(001) surface multiphonon processes at higher beam energies.[22] It is also worthwhile noting that the measured multiphonon excitations are perfectly harmonic up to the seventh overtone, to within experimental error. This provides some clues as to the nature of the interaction of the helium atoms with a surface, as will be discussed later.

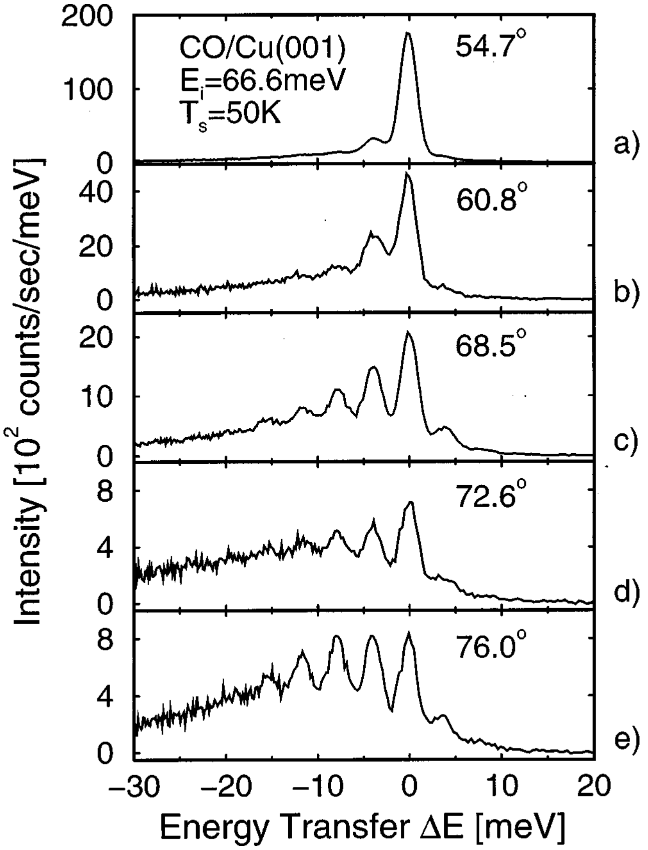

FIG. 3. Several helium time-of-flight spectra, converted to an energy-transfer scale, for a CO coverage of $\Theta_{CO} = 0.028$ on Cu(001) and a range of incident angles θ_i with $\theta_f = \theta_{SD} - \theta_i$. The surface temperature was $T_s = 50$ K and the incident energy was $E_i = 66.6$ meV. Multiple excitations of the T-mode peak at $\Delta E = \pm n \times 4$ meV become dominant features of the spectra as the incident angle is increased.

In addition to the measurements of CO/Cu(001), TOF spectra were obtained for a low coverage ($\Theta_{CO} \approx 0.03$) of CO on Pt(111) under similar scattering conditions. The CO/Pt(111) T-mode frequency was determined in earlier measurements[5,14] to be $\hbar\omega = 6$ meV, 50% higher than that for CO/Cu(001) and thus provides a useful comparison. Fig-

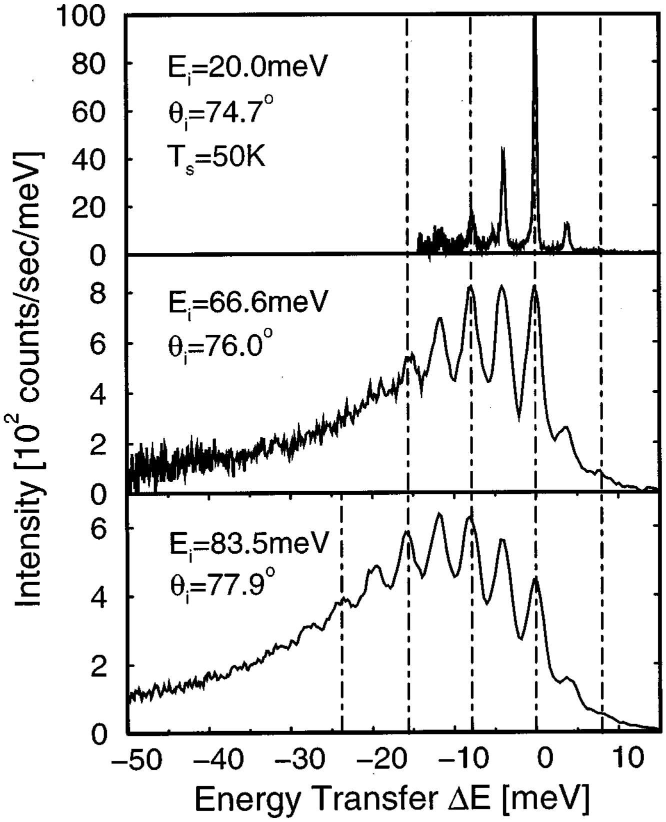

FIG. 4. A series of helium-atom scattering inelastic time-of-flight spectra, converted to an energy-transfer scale, for a CO coverage of $\Theta_{\mathrm{CO}}=0.028$ on Cu(001) and incident energies of $E_i=20.0$, 66.6, and 83.5 meV. The surface temperature was $T_s=50\,\mathrm{K}$ and the incident angle is approximately constant in the range $\theta_i=74.7°-77.9°$. At 20 meV the second overtone of the $\Delta E=-4\,\mathrm{meV}$ T-mode peak at $\Delta E=-12\,\mathrm{meV}$ is just visible, whereas the seventh overtone is observed for an incident energy of 83.5 meV. The substantially increased background at higher incident energies is due to multiphonon excitations of the Cu(001) substrate phonon modes.

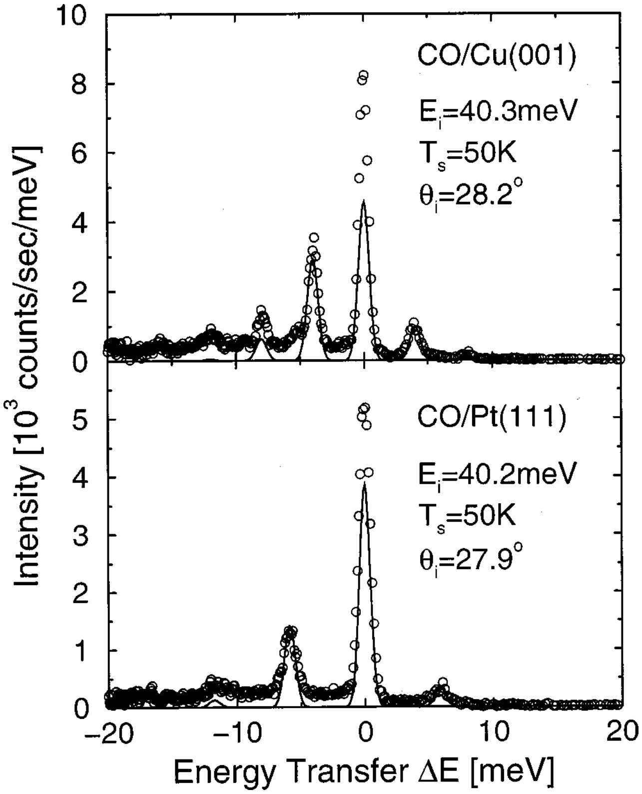

FIG. 5. Comparison between the TOF spectra for helium scattered from CO on Cu(001) and Pt(111). The scattering conditions are nearly identical; the incident energies are 40.3 and 40.2 meV, and the incident angles are $\theta_i=28.2°$ and $\theta_i=27.9°$ for CO/Cu(001) and CO/Pt(111), respectively. The coverage was $\Theta_{\mathrm{CO}}\approx 0.03$ and the surface temperature $T_s=50\,\mathrm{K}$ in both cases, and the spectra have been converted from flight time to energy transfer. Note that the peak width for the CO/Pt(111) T-mode at $\Delta E=-6\,\mathrm{meV}$ is larger than that for CO/Cu(001) due to the shorter vibrational lifetime. The solid curves are the calculations discussed in Sec. V.

ure 5 compares TOF spectra measured under nearly identical scattering and temperature conditions for $\Theta_{\mathrm{CO}}\approx 0.03$ CO on Cu(001) and Pt(111). The spectra for CO/Pt(111) exhibit fewer overtones than those for CO/Cu(001), as expected for the higher vibrational frequency. However, the distribution of intensity with energy transfer (intensity envelope) is similar in both cases, taking into account the larger peak width of the CO/Pt(111) T-mode vibration due to the shorter lifetime[14] compared to CO/Cu(001).[10] Also shown in Fig. 5 as solid curves are the theoretical calculations as discussed below in Sec. V.

IV. THEORY

A. Differential reflection coefficient

An appropriate starting point for a general treatment of inelastic scattering between a projectile and a many-body target is the quantum-mechanical transition rate, or generalized Fermi golden rule, for the projectile to scatter from the initial state of wave vector $\mathbf{k}_i$ to the final state $\mathbf{k}_f$, which is given by[23,24]

$$w(\mathbf{k}_f,\mathbf{k}_i)=\left\langle \frac{2\pi}{\hbar}\sum_{\{n_f\}}\left|\langle n_f,\mathbf{k}_f|\mathcal{T}|\mathbf{k}_i,n_i\rangle\right|^2\delta(\mathcal{E}_f-\mathcal{E}_i)\right\rangle, \tag{1}$$

where $|n_i\rangle$ is the initial many-body state of the unperturbed target, $\Sigma_{\{n_f\}}$ is a summation over all final states of the target, $\mathcal{T}$ is the transition operator, $\mathcal{E}_f$ and $\mathcal{E}_i$ are respectively the final and initial energy of the entire system of target plus projectile, and the angular brackets $\langle\,\rangle$ signify an average over all initial target states. In atom-surface scattering the measured intensities are usually differential reflection coefficients, which are obtained from the transition rate $w(\mathbf{k}_f,\mathbf{k}_i)$ on multiplication by the density of final scattering states as follows:

$$\frac{dR}{d\Omega_f dE_f}=\frac{L^4}{(2\pi\hbar)^4}\,\frac{m^2|\mathbf{k}_f|}{k_{iz}}\,w(\mathbf{k}_f,\mathbf{k}_i), \tag{2}$$

where m is the mass of the projectile atom and k_{iz} is the component of the incident wave vector perpendicular to the surface.

A general expression for the transition rate for the full transition operator can be obtained in the semiclassical limit. This involves making the approximation that the collision is fast in comparison to phonon periods and that it is sufficient to expand the interaction potential through terms linear in the atomic displacements. These approximations have been justified in detail in connection with development of multiphonon exchange in atom-surface scattering, and have been shown to be valid through extensive comparison with experimental measurements.[24–27] The result is the following form for the transition rate:

$$w(\mathbf{k}_f,\mathbf{k}_i)=\frac{1}{\hbar^2}|\tau_{fi}|^2 e^{-2W(\mathbf{k}_f,\mathbf{k}_i)} \times\int_{-\infty}^{+\infty} dt\, e^{-i(E_f-E_i)t/\hbar} e^{Q(\mathbf{k}_f,\mathbf{k}_i;t)}, \tag{3}$$

where $Q(\mathbf{k}_f,\mathbf{k}_i;t)$ is a generalized displacement correlation function and $2W(\mathbf{k}_f,\mathbf{k}_i)=Q(\mathbf{k}_f,\mathbf{k}_i;t=0)$.[27] In the semiclassical approximation of quick collisions, i.e., collision times that are short compared to a vibration period, the time-dependent correlation function $Q(\mathbf{k},t)$ becomes the displacement correlation function

$$Q(\mathbf{k}_f,\mathbf{k}_i;t)\rightarrow Q(\mathbf{k},t)=\langle \mathbf{k}\cdot\mathbf{u}(\mathbf{0})\mathbf{k}\cdot\mathbf{u}(\mathbf{t})\rangle, \tag{4}$$

where $\mathbf{k}=\mathbf{k}_f-\mathbf{k}_i$ is the scattering vector, and the argument of the Debye-Waller factor is

$$2W(\mathbf{k})=Q(\mathbf{k},t=0)=\langle[\mathbf{k}\cdot\mathbf{u}(\mathbf{0})]^2\rangle. \tag{5}$$

In Eq. (3) the energies E_f and E_i are, respectively, the final and initial kinetic energies of the scattered projectile. The factor $|\tau_{fi}|^2$ is the form factor that depends on the nature of the scattering center and the interaction potential. The form factor is discussed in more detail in Sec. IV B.

In the case of a vibrational displacement having only a single dispersionless Einstein mode of frequency ω, Eqs. (3) and (4) can be evaluated together, and the result is a generalized temperature-dependent Poisson series that produces multiphonon overtones.[28] This expression appears as follows:

$$\frac{d^3R(\mathbf{k}_f,\mathbf{k}_i)}{dE_f d\Omega_f}=\frac{m^2}{(2\pi\hbar)^4}\frac{|\mathbf{k}_f|}{k_{iz}}|\tau_{fi}|^2 e^{-2W(\mathbf{k})}e^{-2W_T(\Delta\mathbf{K})} \times\sum_{\alpha=-\infty}^{+\infty} I_{|\alpha|}\left(\frac{\Delta\mathbf{K}^2\hbar}{M_A\omega}\sqrt{n(\omega)[n(\omega)-1]}\right) \times\left(\frac{n(\omega)}{n(\omega)-1}\right)^{\alpha/2}\delta(E_f-E_i-\alpha\hbar\omega), \tag{6}$$

where $I_\alpha(z)$ is the modified Bessel function of order α, $|\tau_{fi}|^2$ is the form factor, $\Delta\mathbf{K}$ is the component of $\mathbf{k}$ parallel to the surface, M_A is the effective mass derived from the normal-mode analysis of the CO adsorbate as shown in Sec. IV C, and $n(\omega)$ is the Bose-Einstein function given by

$$n(\omega)=\frac{1}{e^{\hbar\omega/k_BT_s}-1}. \tag{7}$$

The Debye-Waller factor arising from the contribution of the adsorbate T mode is given by

$$2W_T(\Delta\mathbf{K})=\frac{\hbar\Delta\mathbf{K}^2}{2M_A\omega}\left[n(\omega)+\frac{1}{2}\right], \tag{8}$$

while $2W(\mathbf{k})$ is the contribution to the Debye-Waller factor arising from the substrate modes, which for a Debye model of the substrate vibrations has the familiar high-temperature limit given by

$$2W(\mathbf{k})=\frac{3\hbar^2\mathbf{k}^2T_s}{M_Ck_B\Theta_D^2}, \tag{9}$$

where M_C is the mass of a substrate atom. However, in the calculations presented here we used the fully quantum-mechanical form of Eq. (9), which includes zero-point motion of the substrate lattice.[27] The analysis of the scattering intensity measurements in this manuscript is based primarily on Eq. (6), and we note that this result contains a full treatment of the adsorbate recoil because the zero-point motion is treated correctly throughout.

B. The form factor

In order to calculate the adsorbate multiphonon peak intensities accurately, the choice of a suitable form factor, or adsorbate shape, needs to be considered. In the semiclassical limit, the form-factor amplitude τ_{fi} is given by the transition matrix for scattering by the elastic part of the interaction potential extended off the energy shell,[27] thus permitting the form factors derived from elastic scattering experiments and calculations to be used for the present inelastic scattering calculations. A complete form factor contains all the details of the scattering interaction including multiple scattering from the adsorbate and surface, the He-adsorbate potential, and the He-metal surface potential. These details typically make a full form factor difficult and time consuming to compute.[29] Fortunately, in previous work on the scattering of He atoms from adsorbed CO, it has been shown that both the elastic and inelastic scattering cross sections are determined largely by scattering from the hard repulsive core of the CO. Furthermore, this core is well approximated by a hard hemisphere for the scattering of He from isolated CO on close-packed metal surfaces.[20,21,30]

Using these established ideas, a simple model for the form factor for the present problem can be developed based on the scattering from a hard sphere. In standard treatments, the scattering from an isolated scattering center is described by an asymptotic wave function of the form

$$\Psi_i\rightarrow e^{i\mathbf{k}_i\cdot\mathbf{r}}+\frac{f(\theta,\phi)}{r}e^{ik_ir}. \tag{10}$$

For a hard sphere of radius a, the form factor $f(\theta)$, as a function of the scattering angle θ, is given by the following well-known expression in the Kirchhoff limit $k_ia\rightarrow\infty$,[31]

$$f(\theta) = -\frac{ia}{2}\left\{ i\exp\left(-2ik_i a \sin\frac{\theta}{2}\right) - k_i a\left(\frac{1+\cos\theta}{k_i a \sin\theta}\right) J_1(k_i a \sin\theta)\right\}, \qquad (11)$$

where $J_1(z)$ is the first-order Bessel function. The use of the Kirchhoff approximation is justified for the present case because the incident wave vectors range from roughly 6 to 12 Å^{-1} and the hard-core radius of the He-CO potential is about 2.3 Å; thus $k_i a > 10$ for all incident energies. The first term on the right-hand side of Eq. (11) is called the illuminated face contribution and it produces uniform scattering intensity at all angles, while the second term is the Fraunhofer contribution.

If the adsorbed CO is modeled by a hemisphere on an otherwise flat, mirror surface, then one must account for the possibility of double scattering events involving scattering from the hemisphere plus a reflection with a concomitant phase change of π by the flat surface. This is readily effected by adding to Eq. (11) a second term that accounts for the double scattering processes from the flat surface. For the simplest case of scattering in the sagittal plane, and for a fixed angle θ_{SD} between the incident beam and the detector direction, the scattering form factor becomes

$$f_S = f(\pi - \theta_{SD}) - f(\theta_f - \theta_i), \qquad (12)$$

where θ_i and θ_f are the incident and final scattering angles with respect to the surface normal, respectively.

The form factor corresponding to this model is given by $|\tau_{fi}|^2 \propto |f_S|^2$, which consists of an envelope governed by the Fraunhofer term at small parallel momentum transfer $\Delta\mathbf{K}$ and by the constant illuminated face contribution at large $\Delta\mathbf{K}$. It also contains interference terms called ''reflection symmetry oscillations'' because of their similarity in origin to the symmetry oscillations observed in identical particle scattering.[20]

An even simpler approximation to the form factor is to use only the envelope function, which is given by

$$|\tau_{fi}|^2 \propto \overline{|f_S(\theta)|^2} \propto \left\{1 + \frac{4\mathbf{k}_i^2}{\pi a}\frac{1}{|\Delta\mathbf{K}|^3}\right\}. \qquad (13)$$

This simple form factor combines the two essential features arising from hard-core scattering, which are the Fraunhofer contribution that varies as $|\Delta\mathbf{K}|^{-3}$, and the illuminated face contribution, which is a constant. It is a function of both the final and initial energies through its dependence on the parallel momentum transfer $\Delta\mathbf{K}$. Equation (13) is the form factor that is used in the analysis of the data in Sec. V below.

C. Normal-mode analysis

In order to obtain the effective mass M_A of the CO molecules for each of the vibrational modes a normal-mode analysis for the modes of CO adsorbed on a Cu(001) surface was made. A model adequate for the purposes of the analysis presented here is the simple ball-and-spring model shown in Fig. 6. This model leaves the vertical and horizontal motion of the carbon and oxygen atoms uncoupled. For vertical motion the spring of spring constant k_C^z represents the carbon-metal bond and a second with spring constant k_O^z represents the C-O bond. For the horizontal motion, springs with constants k_C^x and k_O^x connect the carbon and oxygen atoms, respectively, to the surface vertical, and a third k_a^x is an angle-bending spring that tends to restore the carbon and oxygen to a straight-line configuration with respect to the bonding point on the surface.

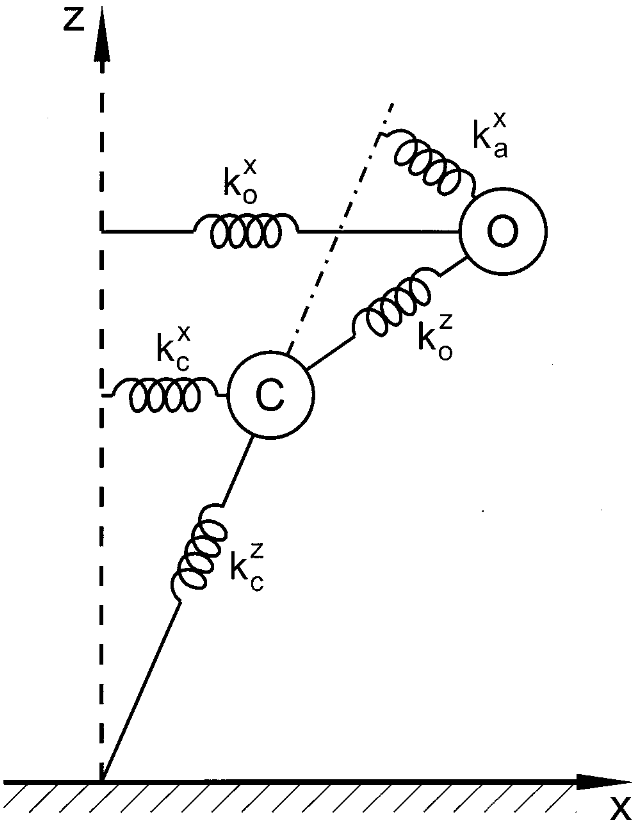

FIG. 6. A schematic diagram of the ''ball-and-spring'' model used for the normal-mode analysis for the vibrations of an isolated CO molecule. For the calculations presented here k_O^x was taken to be zero.

The normal-mode analysis for such a system is straightforward. For the horizontally polarized modes, a satisfactory match of the 4-meV T mode and the 35.3-meV R mode is

TABLE II. Comparison of model calculations with experiment for the isotope shifts of the T- and R-mode frequencies for CO/Cu(001), with respect to the frequency of the $^{12}C^{16}O$ isotopomer, based on the model of Fig. 6.

	T-mode shift (%)		R-mode shift (%)	
Isotope	Expt.[a]	Present calc.	Expt.[a]	Present calc.
$^{12}C^{18}O$	−4.58	−2.64	−0.98	−1.68
$^{13}C^{16}O$	−0.76	−0.28	−3.12	−2.72
$^{13}C^{18}O$	−5.09	−3.76	−3.93	−4.46

[a] Reference 10.

TABLE III. Comparison of model calculations with experiment for the isotope shifts of the *S*-mode and C-O stretch mode frequencies of CO/Cu(001) with respect to the frequency of the $^{12}C^{16}O$ isotopomer, based on our model of Fig. 6.

	S-mode shift (%)		C-O stretch-mode shift (%)	
Isotope	Expt.[a]	Present calc.	Expt.[a]	Present calc.
$^{12}C^{18}O$	−2.08	−3.58		−2.21
$^{13}C^{16}O$	−0.94	−1.61		−2.35
$^{13}C^{18}O$	−3.04	−5.02		−4.63

[a] Reference 10.

obtained with $k_C^x = 620.7\,\mathrm{amu\,meV}^2$, $k_a^x = 6166.8\,\mathrm{amu\,meV}^2$, and $k_O^x = 0$. These two frequencies can also be matched with a large range of values of $k_O^x > 0$ with a concomitant small reduction in the values of the other two constants, but the simplest choice of $k_O^x = 0$ has been used here. This model also predicts the measured isotope shifts in the frequencies well, as shown in Table II.

The relative amplitudes of the carbon and oxygen vibrational amplitudes are expressed in terms of the polarization vectors $e(\beta,\kappa,\nu)$, where β is the Cartesian direction index, κ is an integer denoting the atom, and ν is an integer denoting the mode number. For the low frequency *T* mode this model gives $e(x,\mathrm{O},T)/e(x,\mathrm{C},T) = +1.67$, while for the *R* mode it gives $e(x,\mathrm{O},R)/e(x,\mathrm{C},R) = -0.719$.

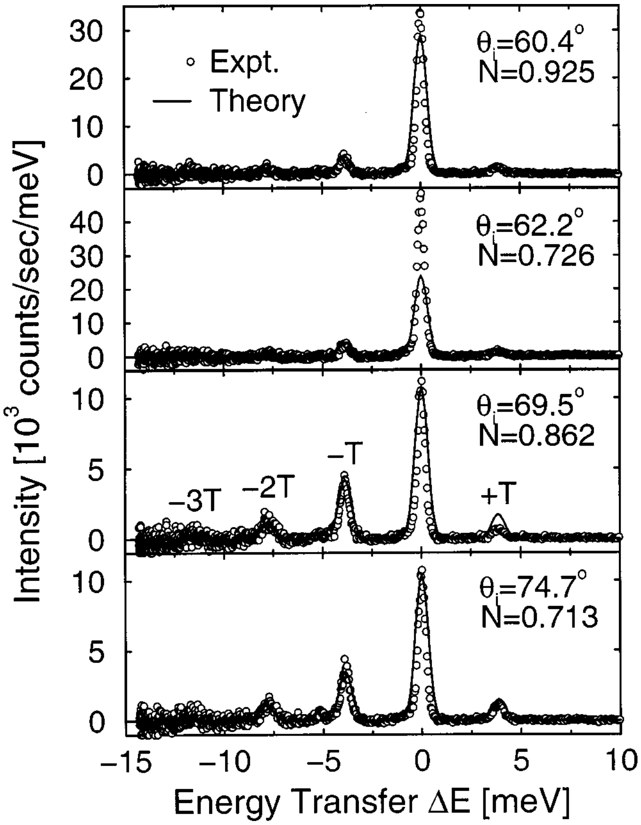

FIG. 7. A series of helium-atom scattering inelastic time-of-flight spectra, converted to an energy-transfer scale, for $\Theta_{CO} = 0.028$ CO on Cu(001) at $T_s = 50\,\mathrm{K}$. The incident energy was 20.0 meV. The incident angles range from $\theta_i = 60.4°$ to $\theta_i = 74.7°$ with $\theta_f = 95.8° - \theta_i$ directed along the Cu(001) [100] azimuth. The experimental points are shown as circles while the solid lines are the results of the theory discussed in the text.

The time-dependent displacement correlation function for a harmonic system such as this is given by

$$\langle u_\kappa^\beta(0)\,u_{\kappa'}^{\beta'}(t)\rangle = \sum_\nu \frac{\hbar}{2N\sqrt{M_\kappa M_{\kappa'}}\,\omega_\nu}\, e(\beta,\kappa,\nu)\,e^*(\beta',\kappa',\nu) \times\{[n(\omega_\nu)+1]e^{-i\omega\nu t}+n(\omega_\nu)e^{+i\omega\nu t}\}, \tag{14}$$

where M_κ is the mass of the κth atom, ω_ν is the frequency of the νth normal mode, and N is the total number of modes. Equation (14) shows that the effect of the polarization on the expression of Eq. (6) for calculating the intensities can be treated through introduction of an effective mass. As discussed above in Sec. IV B, the adsorbed CO molecule can be represented by a hard hemispherical profile, which derives mainly from the hard core of the oxygen atom, on a hard flat surface. This simplifies the calculation because it can be assumed that the only term of Eq. (14) that enters into the calculation of the Einstein mode intensities of Eq. (6) is that for the time-dependent correlation of the oxygen atom with itself. The effective mass of the oxygen atom is $M_A = M_\mathrm{O}/|e(x,\mathrm{O},\nu)|^2$, where M_O is the mass of an oxygen

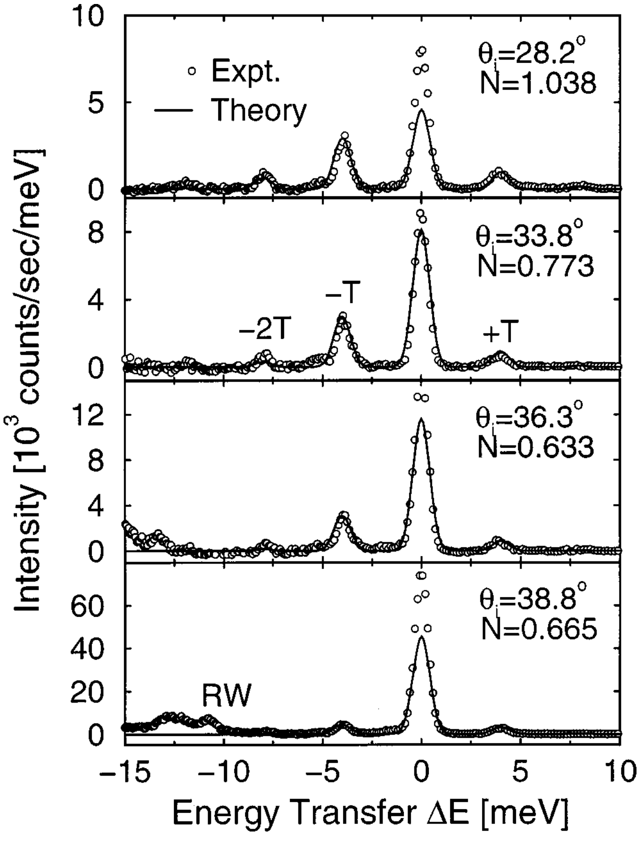

FIG. 8. Same as Fig. 7, except with the incident energy at 40.29 meV, and incident angles from $\theta_i = 28.2°$ to $\theta_i = 38.8°$.

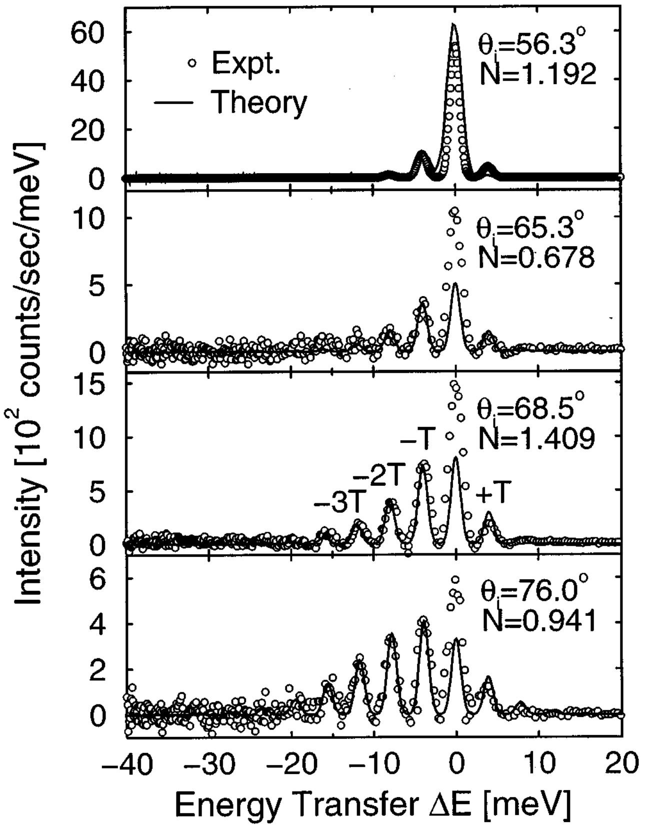

FIG. 9. Same as Fig. 7, except with the incident energy at 66.6 meV, and incident angles from $\theta_i = 56.3°$ to $\theta_i = 76.0°$.

atom, and consequently, the effective mass for the T mode can be taken to be $M_T = M_{\text{O}}/|e(x,\text{O},T)|^2 = 16\,\text{amu}/0.859^2 = 21.7\,\text{amu}$. Similarly, for the R mode an effective mass of $M_R = M_{\text{O}}/|e(x,\text{O},R)|^2 = 16\,\text{amu}/0.584^2 = 46.96\,\text{amu}$ can be obtained.

For the vertically polarized mode, a match to the 42.8-meV S mode and the 258-meV C-O stretch mode is obtained with $k_{\text{C}}^z = 53\,394\,\text{amu meV}^2$ and $k_{\text{O}}^z = 437\,781\,\text{amu meV}^2$. Therefore, the effective mass for the S mode is $M_S = M_{\text{O}}/|e(z,\text{O},S)|^2 = 16\,\text{amu}/0.721^2 = 30.02\,\text{amu}$. The calculated isotope frequency shifts of the S modes and C-O stretch modes are given in Table III.

V. ANALYSIS OF THE DATA

Since in the present work we are mainly interested in the probabilities for inelastic scattering from the adsorbed molecules, the broad substrate multiphonon background under the adsorbate vibrational peaks was subtracted from the experimental TOF spectra to leave just those peaks. This was accomplished by subtracting a smooth curve fitted to the intensity between the adsorbate inelastic peaks from each spectrum. The resulting background-subtracted data is shown in Figs. 7–10.

In order to test the hypothesis that the form factor for inelastic scattering from CO on metal surfaces can be approximated by simple scattering from a hard hemisphere, the calculations using Eq. (6) were first performed for a constant form factor $|\tau_{fi}|^2 = 1$. To compare the results of the calculations, which are a series of energy δ-function peaks, with the experimental measurements, the calculated spectra were broadened with a fixed-width Gaussian function, where the width was fitted to the experimental resolution. These calculations were fitted to the background-subtracted data by multiplying each calculation by a normalization coefficient, where the intensity matching was made, in most cases, using the fundamental energy-loss peak (i.e., the $n = -1$ phonon creation peak). This results in a fit to the experimental data, which, for each individual TOF spectrum, is essentially a zero-parameter fit. This is because the differential reflection coefficient of Eq. (6) with a constant form factor has no adjustable parameters aside from the Debye-Waller temperature appearing in the substrate Debye-Waller factor $2W_S(\mathbf{k})$, which is well known to be $\Theta_D = 220\,\text{K}$ from previous work on clean Cu(001) surfaces.[22]

The resulting normalization coefficients, which contain information about the form factor, are shown for each of the four incident energies in Fig. 11. Presented alongside the coefficient points in Fig. 11 are the form-factor curves derived using Eq. (13) and a radius of $a = 2.3\,\text{Å}$ (solid lines). This value of the radius is well established from previous investigations of the elastic scattering of He from CO on Cu(001) and other metal substrates[21] and, consequently, a cannot be considered to be a freely adjustable parameter. The simple form factor given by Eq. (13) matches the trend of the normalization points quite well for all four incident energies.

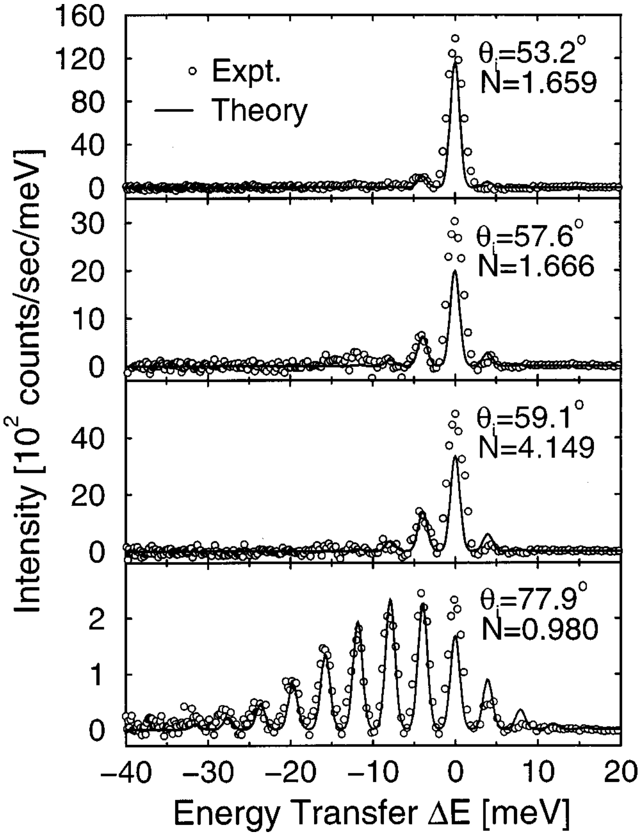

FIG. 10. Same as Fig. 7, except with the incident energy at 83.4 meV, and incident angles from $\theta_i = 56.3°$ to $\theta_i = 76.0°$.

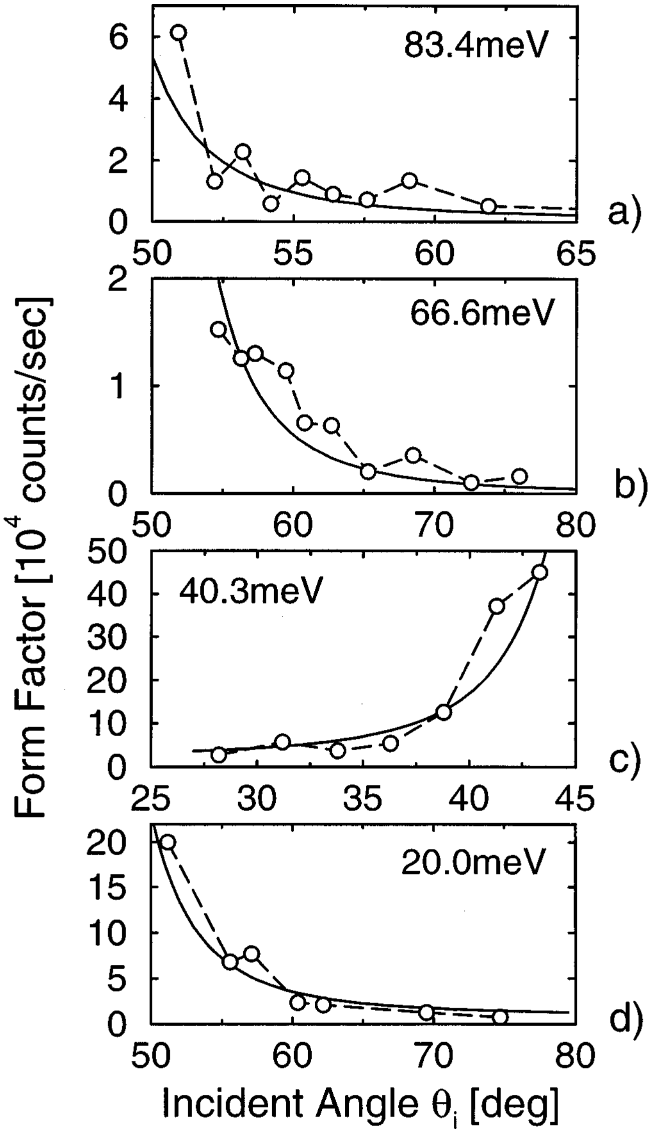

FIG. 11. The experimentally obtained intensity of the $n=-1$ CO/Cu(001) *T*-mode phonon creation peak compared with the form factor of Eq. (13) for the incident energies (a) 83.4 meV, (b) 66.6 meV, (c) 40.3 meV, and (d) 20.0 meV. The experimental intensity is plotted as circles and the solid line is the theoretical form factor for a hard-core radius of $a=2.3$ Å.

It is seen that with scattering at incident angles near the specular condition at $\theta_i=47.9°$ the intensity rises sharply due to the $|\Delta\mathbf{K}|^{-3}$ term at small $\Delta\mathbf{K}$ in the form factor, while for large incident angles the intensity saturates to a smaller constant value that can be attributed to the illuminated face contribution from hard-core scattering. Thus, the observed angular intensity dependences are well represented by the form factor in Eq. (13), justifying its use together with Eq. (6) to simulate the TOF spectra including the momentum-transfer dependences of the intensities.

The results of the complete calculations are shown in Figs. 7–10 (solid lines). In the process of this final calculation with the new form factor it was still found to be necessary to multiply each calculated curve by a renormalization factor *N* close to unity in order to obtain the best fit. The need for this final renormalization is obvious from Fig. 11 because, although the calculated form factor of Eq. (13) follows the observed intensities quite well, the points are scattered about the theoretical curve. The value of the final renormalization constant is shown in each TOF plot. It is seen that these final calculations with the form factor of Eq. (13) agree rather well with all of the TOF experimental data measured.

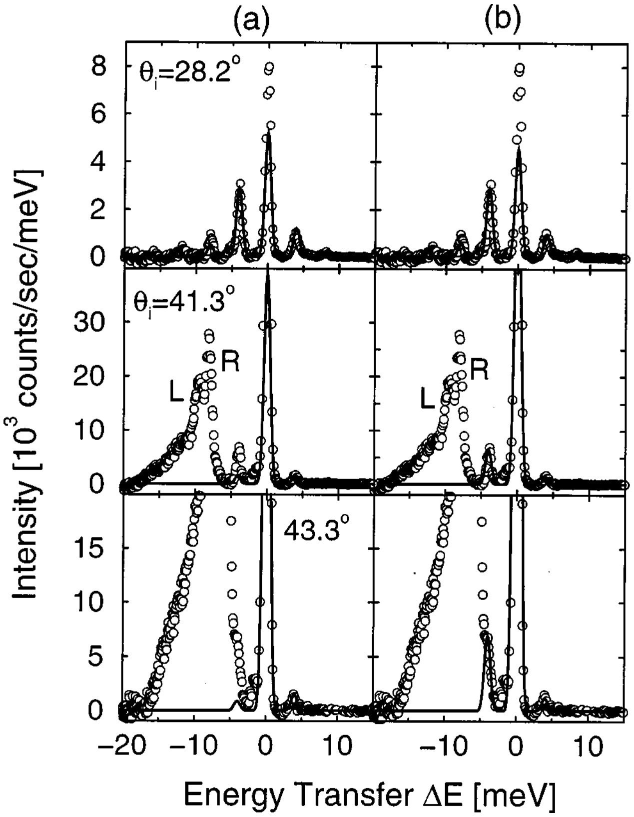

FIG. 12. Comparison of the calculated inelastic multiphonon intensity (thick solid line) with experimental data (circles) for $E_i=40.29$ meV and selected incident angles. (a) shows the results of the calculations without including the scattering form factor of Eq. (13) while (b) shows the same calculations including this factor. At $\theta_i=28.2°$, which is far from specular conditions, the form factor is seen to have little effect. However, at $\theta_i=41.3°$ and 43.3°, which are close to specular and where the Fraunhofer term is dominant, the form factor has an important effect in bringing the calculated intensities for the inelastic overtone peaks into agreement with experiment. The two peaks marked L (longitudinal resonance) and R (Rayleigh mode) arise from the substrate vibrations.

The reason for the residual fluctuations of the inelastic intensities compared with those calculated using the simple form factor is well understood: The characteristic signature of scattering from an isolated adsorbate, whether elastic or inelastic, is a supernumerary rainbow oscillation in the differential reflection coefficient caused by multiple scattering between the adsorbate and the surface substrate.[18,20,21,30] These oscillations are ''reflection symmetry oscillations'' and they are most easily observed in experiments that follow the intensity of a single selected multiquantum overtone peak as a function of parallel momentum transfer $\Delta\mathbf{K}$. They also affect the measured results in this current set of experimental measurements. However, because the current observations were taken at rather widely separated values of incident angles, the measurements are not sufficiently dense to exhibit these oscillations. The small differences appearing in Fig. 11 are clearly due to these oscillations about the envelope function given by Eq. (13), which explicitly excludes these reflection symmetry oscillations.

In Figs. 7–10 it is apparent that often the experimentally measured zero-loss peak is substantially larger than the calculation. This is because contributions to this peak come also from other sources, for example, the diffuse elastic scattering from defects and other impurities on the surface.

The importance of the form factor is illustrated in Fig. 12, which shows TOF spectra for $E_i = 40.29$ meV at three different incident angles. The left-hand panels show the background-corrected data together with calculations using a constant form factor $\tau_{fi}=1$, while the right-hand panels show the same data with calculations obtained with the form factor given by Eq. (13). The two peaks in the experimental data marked L and R are, respectively, the longitudinal resonance and the Rayleigh mode arising from the substrate vibrations. At the incident angle of $\theta_i = 28.2°$, which is far from the specular position and at which the parallel momentum transfers for all observable overtone peaks are rather large [and hence the form factor of Eq. (13) is nearly constant], there is little difference between the two calculations. However, for the two other incident angles that are much closer to specular, the values of $\Delta\mathbf{K}$ are much smaller and there is a large difference between the two calculations because the $|\Delta\mathbf{K}|^{-3}$ term in the form factor has a big effect and varies strongly from peak to peak. However, as shown in the right-hand panel of Fig. 12, when the form factor of Eq. (13) is included in the differential reflection coefficient, the results agree well with experiment. This agreement is important confirmation of the fact that Fraunhofer-like scattering from the hard repulsive molecular core is the most important term in the form factor describing inelastic scattering from adsorbed CO.

The applicability of the present theoretical approach was further tested by comparing the calculations obtained with Eqs. (6) and (13) for CO/Cu(001) with CO/Pt(111). The T-mode frequency of CO/Pt(111) is $\hbar\omega = 6$ meV, 50% higher than that for CO/Cu(001), thus providing a useful comparison, as shown in Fig. 5 for two TOF spectra measured for similar scattering conditions. As for CO/Cu(001), the present theoretical model accurately describes the intensity ratio between the observed inelastic peaks, which, for these particular scattering conditions, are the fundamental and first-overtone energy-loss peaks and the fundamental energy-gain (phonon-annihilation) peak of the 6-meV T mode. The good quality of the fit provides additional support for the present theoretical model.

VI. PREDICTIONS FOR THE *R* AND *S* MODES

In the present experimental measurements, and in previous investigations,[5,6,10,11,30] no evidence for excitation of the R or S modes has been reported using He-atom scattering from CO adsorbates on either Cu or Pt surfaces. It is of interest to examine the question of why this is the case with the present theoretical model in order to see if experimental conditions can be predicted under which these two modes might be observed.

Including the R and S modes in the theoretical model of Eq. (6) is relatively straightforward. Since these modes have frequencies considerably larger than the T mode, it is expected that their intensities will be small and only the first-order energy-loss contribution needs to be included, which is equivalent to calculating these intensities in a first-order Born approximation. However, higher-order overtones, and even cross-term contributions involving the simultaneous exchange of combinations of R-, S-, and T-mode quanta, are readily calculated within this formalism. The differential reflection coefficient for the scattering, including only the first-order contributions for the R and S modes, is

$$\begin{aligned}\frac{d^3R(\mathbf{k}_f,\mathbf{k}_i)}{dE_f d\Omega_f} = {} & \frac{m^2}{(2\pi\hbar)^4}\frac{|\mathbf{k}_f|}{k_{iz}}|\tau_{fi}|^2 e^{-2W_T(\Delta\mathbf{K})}e^{-2W_R(\Delta\mathbf{K})}e^{-2W_S(k_z)}e^{-2W(\mathbf{k})}\Bigg\{\sum_{\alpha=-\infty}^{+\infty} I_{|\alpha|}\left(\frac{\Delta\mathbf{K}^2\hbar}{M_A\omega}\sqrt{n(\omega)[n(\omega)-1]}\right) \\ & \times\left(\frac{n(\omega)}{n(\omega)-1}\right)^{\alpha/2}\delta(E_f-E_i-\alpha\hbar\omega)+I_1\left(\frac{\Delta\mathbf{K}^2\hbar}{M_R\omega_R}\sqrt{n(\omega_R)[n(\omega_R)-1]}\right)\left(\frac{n(\omega_R)}{n(\omega_R)-1}\right)^{-1/2}\delta(E_f-E_i+\hbar\omega_R) \\ & +I_1\left(\frac{k_z^2\hbar}{M_S\omega_S}\sqrt{n(\omega_S)[n(\omega_S)-1]}\right)\left(\frac{n(\omega_S)}{n(\omega_S)-1}\right)^{-1/2}\delta(E_f-E_i+\hbar\omega_S)\Bigg\},\end{aligned} \tag{15}$$

where $\exp\{-2W_R(\Delta\mathbf{K})\}$ is the contribution to the Debye-Waller factor arising from the R mode, $\exp\{-2W_S(\Delta\mathbf{K})\}$ is the contribution to the Debye-Waller factor arising from the S mode, and $\exp\{-2W_T(\Delta\mathbf{K})\}$ and $\exp\{-2W(\mathbf{k})\}$ are, as before, the contributions to the Debye-Waller factor arising from the T mode and substrate modes, respectively.

Using the parameters for the existing experimental results, namely, a total scattering angle of $\theta_{SD} = 95.8°$ and incident energies up to 100 meV, Eq. (15) together with Eq. (13) does not predict significant inelastic peak intensities for either the R or S modes, in agreement with the experimental observations. In fact, from the form of Eq. (15) it is clear why the high-energy modes have such small scattering intensities. First, the larger frequencies for ω_R and ω_S make the arguments of both the Bessel function and the value of the Bose-Einstein factor considerably smaller, making the intensity much smaller than that for the *T* mode despite the coupling of the *S* mode to the larger perpendicular component of the momentum transfer k_z. Second, for the *R* mode, as discussed in Sec. IV C above, the normal-mode analysis gives a vibrational amplitude for the oxygen atom vibration of $e(x,\mathrm{O},R)/e(x,\mathrm{C},R) = -0.72$, as opposed to a value of $e(x,\mathrm{O},T)/e(x,\mathrm{C},T) = 1.7$ for the *T* mode. For the *R* mode this translates into a large effective mass for the oxygen atom $M_R = M_\mathrm{O}/|e(x,\mathrm{O},R)|^2 = 16\,\mathrm{amu}/0.584^2 = 46.96\,\mathrm{amu}$, significantly reducing the calculated intensity and the contribution of the Debye-Waller factor. Similarly, as expected, it is found that the effective mass for the *S* mode is close to the mass of the whole CO molecule, about twice the mass of an oxygen atom, $M_S = M_\mathrm{O}/|e(z,\mathrm{O},S)|^2 = 16\,\mathrm{amu}/0.721^2 = 30.78\,\mathrm{amu}$, which also tends to make the intensity of this mode smaller.

In particular, for the *R* mode, as noted earlier, the associated momentum transfer is the parallel component, while for the *S* mode it is the perpendicular component. This has two important effects: First, the conditions in which the *R* mode would produce large intensities, i.e., large parallel momentum transfers, will also be very favorable for the exchange of *T*-mode phonons. Thus, the lower frequency and smaller effective mass for the *T* mode make it dominant. Further, the Debye-Waller contribution due to the *T* mode will make both the *R*- and *S*-mode contributions small. This effect will make it particularly difficult to observe the *R* mode, and probably explains why it has not yet been reported in He-atom experiments.

The perpendicular momentum transfer k_z associated with the *S* mode should, on the other hand, help to make its intensity large. In the experiments shown in Figs. 7–10 the parallel momentum transfers are small and range up to 3–4 Å^{-1}, while the perpendicular components are typically larger than 10 Å^{-1}. Since these momentum transfers enter as squared terms in Eq. (15) this difference is substantially magnified. Thus, it would, at first, appear that the *S*-mode scattering intensity should be most observable under conditions in which the perpendicular momentum transfer is maximized and simultaneously the parallel momentum is minimized so that the *T*-mode contribution to the Debye-Waller attenuation is small. For the present experiments, this would correspond to incident angles near specular and a small angle θ_{SD} between the incident beam and detector, rather than the present angle of 95.8°.

A number of calculations were, consequently, made using Eq. (15) for realistic experimental geometries, which were anticipated to show the *S* mode for CO/Cu(001). Figure 13 shows the predicted TOF spectra for incident helium-atom energies ranging from 50 to 100 meV and a small incident angle of $\theta_i = 22.5°$, with the detector placed at $\theta_f = 2.5°$, making $\theta_{SD} = 25°$. The calculations are scaled to represent a realistic incident beam flux by interpolating between the normalization factors for the experimental data given in Figs. 7–10. Thus, the calculated intensities shown in Fig. 13 are expected to represent realistic values realized for the present experimental apparatus with a smaller total scattering angle.

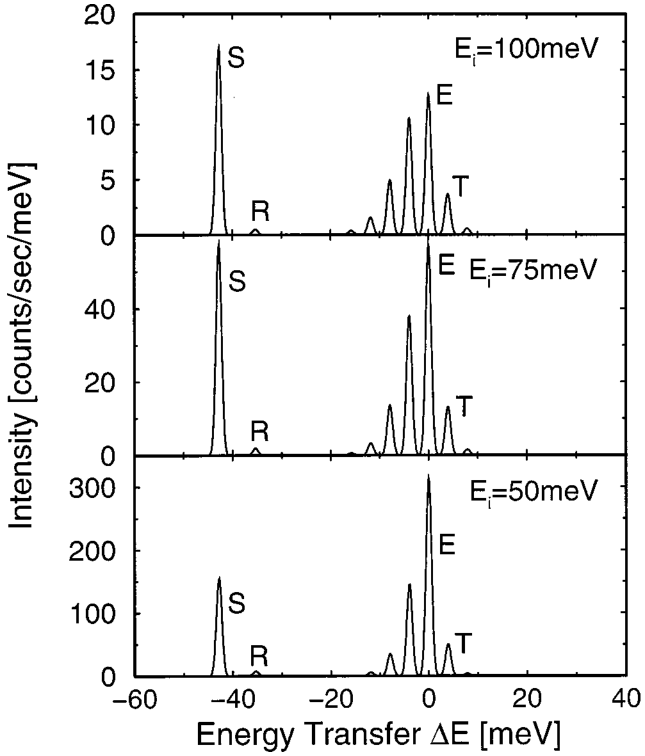

FIG. 13. A series of calculated helium-atom scattering inelastic spectra using realistic incident beam fluxes for isolated CO on Cu(001) at $T_s = 50\,\mathrm{K}$. The incident angle is $\theta_i = 22.5°$ and the scattering angle is $\theta_f = 2.5°$, corresponding to $\theta_{SD} = 25°$. The incident energies range from 50 to 100 meV. In addition to the *T*-mode multiphonons at $\Delta E \approx \pm n \times 4\,\mathrm{meV}$, at $\Delta E \approx -35\,\mathrm{meV}$ the contribution of the *R* mode appears, and at $\Delta E \approx -43\,\mathrm{meV}$ the contribution of the *S* mode is observed as well.

Under these conditions the *S*-mode peak at $\Delta E = -43\,\mathrm{meV}$ exhibits a total integrated intensity relative to that of the sum of all in-plane *T*-mode overtones ranging from ≈25% at $E_i = 50\,\mathrm{meV}$ to ≈50% at $E_i = 100\,\mathrm{meV}$. On the other hand, the *R*-mode peak, while clearly visible in the calculations, is no larger than the smallest of the non-negligible *T*-mode peaks. As the incident energy increases from 50 to 100 meV the relative intensities of both the *T*-mode and the *S*-mode peaks increase, but for the *R* mode this increase is much less apparent. Note that the widths of the *S*- and *R*-mode peaks in Fig. 13 were chosen to be the same as that of the *T*-mode overtones, which is approximately the energy resolution of the experiment.

Consequently, we can conclude from the calculations that the *S* mode should be observable under conditions in which the parallel momentum transfer is small and the perpendicular momentum transfer is large, i.e., high incident energies and small incident and final scattering angles. However, if the parallel momentum transfer is non-negligible, even if it is significantly smaller than the perpendicular momentum transfer, the Debye-Waller factor due to the *T* mode will be so small as to severely damp out the *S*-mode intensity. The *R* mode, on the other hand, is predicted to be difficult to observe under almost all experimental conditions because large parallel momentum transfers are needed. Thus, as a result of the high frequency and higher effective mass of the R mode and the significant T-mode multiphonon creation for large ΔK, the Debye-Waller factors for the R mode are small, resulting in lower intensities.

VII. CONCLUSIONS

In the present paper, detailed experimental results for the multiple excitation of the parallel vibrational modes of CO adsorbed on Cu(001) and Pt(111) have been presented. The angular distribution of intensity into the multiphonon peaks was described in a simple way by a comprehensive scattering theory using only the most basic aspects of the interaction between helium atoms and the adsorbed molecules on the surface. From a detailed comparison between the experimental results and theoretical calculations, the following conclusions can be drawn:

(1) The multiphonon intensity distribution is described well using a self-consistent theory that is, essentially, a generalized temperature-dependent Poisson distribution multiplied by a form factor that describes the interaction between the probe particle and the surface. It was shown that, for a large range of scattering conditions, the form factor can be reduced to a simple hard-core profile and, in addition, that the overall features of the scattering can be reproduced by ignoring multiple scattering. Furthermore, because the details of the hard-core profile had been determined in earlier elastic scattering measurements, there were no freely adjustable parameters and the calculations could be performed *independently* of the present experimental results. There are no freely adjustable parameters because the theoretical results depend only on the masses, the mode frequency, the hard-core radius of the He-CO interaction potential, and the substrate Debye temperature, all of which are well established by other independent experiments. As an additional point, the results depend only very slightly on the substrate Debye temperature because the substrate Debye-Waller factor has very little effect.

(2) The effective mass of the molecule for each vibration must be taken into account. For the present cases of CO/Cu(001) and CO/Pt(111) this was achieved using a ball-and-spring model and fitting the force constants to the known isotope shift measurements. The good fit of the scattering theory to the experimental data showed, in addition, that the helium atoms probe the motion of the oxygen atom, which sits furthest out from the metal surface.

(3) The overtones of the T mode for CO/Cu(001) observed with HAS are equally spaced in energy and exhibit no observable increase in peak width with overtone number. In particular, the $n=-8$ T-mode peak or seventh overtone was observed at an energy loss of $\Delta E=-32\,\text{meV}$. Since other experiments have shown that the CO/Cu(001) lateral potential is quite anharmonic and the diffusion barrier is only about 30 meV,[10] the observed multiphonon excitations do not appear to be those of single molecules. This can be understood by considering that, just as in the case of helium diffraction, single helium atoms interact with an area of the surface corresponding to the coherence width of the helium wave packets, which is equivalent to the coherence width of the helium beam. With use of a typical coherence width of 300 Å and the experimental CO coverage of $\Theta_{\text{CO}}=0.03$, it can be seen that each helium atom interacts with about 330 CO molecules. Thus, even though the CO molecules are isolated, in the sense that there is no significant multiple scattering between them, this work provides strong evidence that the multiple overtone energy transfer clearly must be a collective quantum effect. In other words, these overtones are true ''phonon'' modes, i.e., they are collective oscillations involving a very large number of adsorbed CO molecules. Such a collective and coherent interpretation of the inelastic phonon loss spectra is consistent with a coherent quantum picture of the elastic diffraction of He atoms, and indeed small first-order diffraction peaks due to the two-dimensional lattice gas nature of the rarefied CO coverage are observed, just as they have been observed in previous experiments on low coverages of CO on metal surfaces.[20]

However, the present interpretation of the multiphonon inelastic exchange as a coherent phenomenon involving many CO adsorbates is clearly open to objections. Alternative explanations, not invoking a coherent scattering event, can be developed on assumptions that the incoming He atom scatters with only a single CO adsorbate and exchanges the energy with only that one adsorbate, or the incoming He atom scatters successively with several CO adsorbates in a multicollision process and exchanges energy with several adsorbates.

The main argument presented here against a localized interaction with a single CO adsorbate is the absence of any observable anharmonicity in the measured overtone spectra even up to large overtone numbers. A secondary argument is that coherence in the incoming beam over distances encompassing large numbers of CO adsorbates is clearly evidenced by the observation of small diffraction peaks. With respect to the question of anharmonicity, the barrier for CO diffusion on this same Cu(001) surface has been measured to be $31\pm 10\,\text{meV}$,[10] which is comparable to or even smaller than the $n\approx 8$ quanta or $\Delta E\approx 32\,\text{meV}$ of energy loss observed here under favorable incident conditions. However, the measurements of the dynamic diffusion barrier that were carried out at temperatures of over 100 K may not represent well the actual many-body potential well of the adsorbed CO at the lower temperature of 50 K used in the present measurements. Clearly, it is conceptually incorrect to discuss the diffusion barrier in terms of a static potential due to the substrate, especially in a case in which the barrier is small. The thermal diffusion barrier is the transition point along an effective reaction coordinate in the multidimensional space of very many degrees of freedom of the CO and its surrounding Cu atoms. Thus the diffusion barrier may correspond to a very unusual configuration such as large thermal excursions of surrounding substrate Cu atoms. Such configurations may be less probable during a scattering event, especially one at lower temperatures. Thus it is possible that mobility of the CO after direct impact is quite different from that observed in thermal diffusion, an argument in favor of nearly harmonic and large-quantum-number energy transfers to a single adsorbate. However, in contradiction to this argument, there are He-atom scattering measurements of both the

T-mode overtone linewidths and the small shift in mode frequency as a function of surface temperature that show that this same CO/Cu(001) system exhibits some anharmonicity even at temperatures as low as the 50 K used here.[32]

Multicollision processes, in which the incoming He projectile makes successive semiclassical collisions with several CO adsorbates and exchanges only a small number of quanta at each collision, are a possible explanation for the absence of observed anharmonicity in the overtone peaks. However, the large average distance of greater than 10 Å between CO adsorbates at the low coverages used here makes such collisions unlikely. The nearly linear increase in the inelastic *T*-mode intensities up to CO coverages of approximately 6%, as exhibited in Fig. 2, is consistent with the assumption of isolated scattering centers with no multiple collisions. The nonlinear coverage dependence of the inelastic *T*-mode intensities at coverages greater than 6% implies that multiple scattering is occuring only at coverages greater than those used in this work. The absence of multiple collisions is also confirmed by independent measurements and calculations of the elastic differential scattering cross sections for He-atom scattering from similar low-coverage CO/Cu(001) surfaces[21,30] and by earlier work on the elastic total cross sections of isolated CO adsorbed on a Pt(111) substrate.[17,33] These earlier calculations of both differential and total cross sections for He-atom scattering from isolated CO adsorbates on Cu(001) agreed well with the measured cross sections at low adsorbate coverages comparable to those used here, and the comparison gives no evidence for multiple collisions of He with more than one CO. The calculated differential cross sections provide a way of estimating the multiple-collision intensities in terms of successive single collisions, and such estimates indicate that the multiple scattering contribution to the elastic cross section is significantly less than 1%. Since the same hard-core scattering interaction is predominantly involved in both the elastic and inelastic scattering processes,[21,30] it appears unlikely that multiple collisions play a significant role in the inelastic scattering.

(4) The present theory has shown why, under the present experimental conditions, the *S*- and *R*-mode vibrations of adsorbed CO have not been observed to date even for experiments using incident energies considerably higher than the energy loss associated with these modes. It was found that, due to the near 90° geometry of current HAS experiments, the ratio of parallel to perpendicular momentum transfer favors the creation of *T*-mode multiphonons at the expense of the higher-frequency modes. It was shown that small incident and total scattering angles are more favorable for *S*-mode phonon creation, whereas the *R* mode is expected to be weak under almost all scattering conditions, and probably undetectable.

It is also of great interest to note that the present theoretical formalism provides a very clear method for the determination of the mode characteristics of vibrations with unknown polarizations, provided an appropriate form factor is known. For isolated molecules, such as CO at low coverages, the hard hemispherical potential leads to a form factor that depends on the parallel momentum transfer according to $|\Delta K|^{-3}$ for intermediate values $0.3\,\text{Å}^{-1} \lesssim |\Delta K| \lesssim 2\,\text{Å}^{-1}$. For low surface temperatures the Debye-Waller terms in Eq. (6) tend to unity and the single *T*-mode phonon creation can be described by the I_1 modified Bessel function, which is proportional to $|\Delta K|^2$. Thus, for intermediate parallel momentum transfers the fundamental *T*-mode intensity should follow a roughly $|\Delta K|^{-1}$ dependence. For a total scattering angle close to 90° the perpendicular momentum transfer k_z varies little with ΔK and the *S*-mode intensity is, consequently, dominated by the form-factor term in Eq. (15), leading to a $|\Delta K|^{-3}$ dependence for intermediate $|\Delta K|$. Thus, the fundamental *S*-mode peak intensities are expected to show a strong decrease in intensity as $|\Delta K|$ is increased away from specular, whereas the *T*-mode dependence is anticipated to be much weaker.

Finally, we would like to point out that the theoretical model used to analyze the present experimental results is not limited to the scattering of helium from specific adsorbate systems. The ease of application of this approach means that it can be used to predict the interactions of other molecules with different adsorbates for a Maxwell-Boltzmann distribution of incident energies that are typical for realistic systems.

ACKNOWLEDGMENTS

We would like to thank J. P. Toennies for support, encouragement, and stimulating discussions during the course of this work. One of the authors (J.R.M.) would like to thank the Max Planck Institut für Strömungsforschung for hospitality during the course of this work. This work was supported by the National Science Foundation under Grant No. DMR-9726229 and by the Department of Energy under Grant No. DE-FG02-98ER45704.

---

[1] S. C. Saxena and R. K. Joshi, *Thermal Accommodation and Adsorption Coefficients of Gases*, CINDAS Data Series on Material Properties, edited by C. Y. Ho (Hemisphere, New York, 1989).

[2] H. Legge, J. P. Toennies, and J. R. Manson, J. Chem. Phys. **110**, 8767 (1999).

[3] F. Hofmann, J. R. Manson, and J. P. Toennies, Surf. Sci. **349**, L184 (1996).

[4] B. F. Mason and B. R. Williams, Surf. Sci. **130**, 295 (1983).

[5] A. M. Lahee, J. P. Toennies, and Ch. Wöll, Surf. Sci. **177**, 371 (1986).

[6] J. Ellis, J. P. Toennies, and G. Witte, J. Chem. Phys. **102**, 5059 (1995).

[7] A. Siber, B. Gumhalter, J. Braun, A. P. Graham, M. F. Bertino, J. P. Toennies, D. Fuhrmann, and Ch. Wöll, Phys. Rev. B **59**, 5898 (1999).

[8] C. J. Hirschmugl, G. P. Williams, F. M. Hoffmann, and Y. J. Chabal, Phys. Rev. Lett. **65**, 480 (1990).

[9] C. M. Truong, J. A. Rodriguez, and D. W. Goodman, Surf. Sci. Lett. **271**, L385 (1992).

[10] A. P. Graham, F. Hofmann, J. P. Toennies, G. P. Williams, C. J.

Hirschmugl, and J. Ellis, J. Chem. Phys. **108**, 7825 (1998).

[11] A. P. Graham, F. Hofmann, and J. P. Toennies, J. Chem. Phys. **104**, 5311 (1996).

[12] E. Schweizer, B. N. J. Persson, M. Tüshaus, D. Hoge, and A. M. Bradshaw, Surf. Sci. **213**, 49 (1989).

[13] H. Steininger, S. Lehwald, and H. Ibach, Surf. Sci. **123**, 264 (1982).

[14] A. P. Graham and J. P. Toennies, Europhys. Lett. **42**, 449 (1998).

[15] J. P. Toennies, in *Surface Phonons*, edited by W. Kress and F. W. de Wette, Springer Series in Surface Sciences (Springer, 1991), Vol. 21, p. 111.

[16] B. Poelsema and G. Comsa, in *Scattering of Thermal Energy Atoms from Disordered Surfaces*, Springer Tracts in Modern Physics (Springer, Berlin, 1989), Vol. 115, p. 1.

[17] B. Poelsema, S. T. de Zwart, and G. Comsa, Phys. Rev. Lett. **49**, 578 (1982); **51**, 522 (1983).

[18] M. Bertino, J. Ellis, F. Hofmann, J. P. Toennies, and J. R. Manson, Phys. Rev. Lett. **73**, 605 (1994).

[19] J. Braun, A. P. Graham, F. Hofmann, W. Silvestri, J. P. Toennies, and G. Witte, J. Chem. Phys. **105**, 3258 (1996).

[20] A. M. Lahee, J. R. Manson, J. P. Toennies, and Ch. Wöll, Phys. Rev. Lett. **57**, 471 (1986); J. Chem. Phys. **86**, 7194 (1987).

[21] A. P. Graham, F. Hofmann, J. P. Toennies, and J. R. Manson, J. Chem. Phys. **105**, 2093 (1996).

[22] F. Hofmann, J. R. Manson and J. P. Toennies, J. Chem. Phys. **101**, 10155 (1994).

[23] L. S. Rodberg and R. M. Thaler, *Quantum Theory of Scattering* (Academic, New York, 1967).

[24] J. R. Manson, Phys. Rev. B **43**, 6924 (1991).

[25] M. F. Bertino, J. R. Manson, and W. Silvestri, J. Chem. Phys. **108**, 10 239 (1998).

[26] R. Brako and D. M. Newns, Phys. Rev. Lett. **48**, 1859 (1982); Surf. Sci. **123**, 439 (1982).

[27] J. R. Manson, Comput. Phys. Commun. **80**, 145 (1994).

[28] J. R. Manson, Phys. Rev. B **37**, 6750 (1988).

[29] D. Lemoine, J. Chem. Phys. **101**, 4343 (1994).

[30] B. H. Choi, K. T. Tang, and J. P. Toennies, J. Chem. Phys. **107**, 1631 (1997); **107**, 9437 (1997).

[31] P. M. Morse and H. Feshbach, *Methods of Theoretical Physics* (McGraw-Hill, New York, 1953), p. 1554.

[32] A. Graham, F. Hofmann, and J. P. Toennies, J. Chem. Phys. **104**, 5311 (1996).

[33] H. Jónsson, J. H. Weare, and A. C. Levi, Phys. Rev. B **30**, 2241 (1984).